Constructing Conjugated Microporous Polymers Containing the Pyrene-4,5,9,10-Tetraone Unit for Energy Storage

Mohamed Gamal Mohamed,* Swetha V. Chaganti, Santosh U. Sharma, Maha Mohamed Samy, Mohsin Ejaz, Jyh-Tsung Lee, Kan Zhang, and Shiao-Wei Kuo*
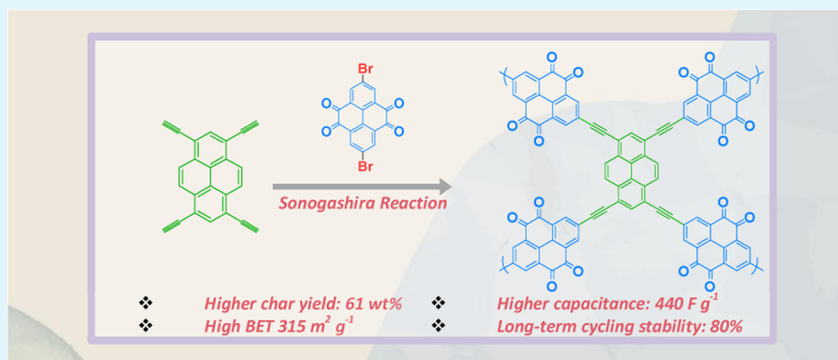
Read Online

ACCESS | Metrics & More | Article Recommendations | Supporting Information

ABSTRACT: In this work, we reported the rational design and synthesis of two pyrene-4,5,9,10-tetraone (PT)-linked conjugated microporous polymers (PT-CMPs) as organic electrode precursors in energy storage applications, which were prepared through the Sonogashira polycondensation reaction of ethynyl pyrene (Py-T)/tetraphenylethene (TPE-T) as common units with brominated pyrene tetraene (PT-Br$_2$) as a redox-active unit. We employed microscopic, spectroscopic, and N$_2$ adsorption/desorption isotherm analyses to investigate the thermal stability, molecular structure, and porosity properties of both newly obtained PT-CMPs. Thermogravimetric analysis (TGA) revealed that both synthesized PT-CMPs feature moderate thermal stability. TheP-PT-CMP exhibited a high BET surface area of up to 300 m^2 g^{-1} and a total pore volume was 0.34 cm^3 g^{-1}, based on N$_2$ sorption analyses. Notably, the P-PT-CMP framework displayed a very high capacitance up to 400 F g^{-1} with superior capacitance stability up to 80% over 5000 cycles at 10 A g^{-1} according to the supercapacitor performance. In addition, we have evaluated the electrochemical performance of a symmetric coin supercapacitor, showing great potential for real-life applications in electrical energy storage (EES).

KEYWORDS: pyrene-4,5,9,10-tetraone, tetraphenylethene, Sonogashira reaction, conjugated microporous polymers, supercapacitor

1. INTRODUCTION

Energy shortages and resource consumption that endanger the environment have heightened our awareness of developing efficient and sustainable energy storage technologies.[1−10] Electrochemical techniques for energy storage technology have been essential in addressing energy crises.[4,11−15] Supercapacitors (SCs) are potential energy storage devices due to their high-rate performance, cycle stability, power density, and environmentally friendly nature.[16−20] These favorable properties also make SCs suitable for other applications, including wind turbines, automobiles, and biological defibrillators.[21−30] SCs have been grouped into pseudocapacitors and electrochemical double-layer capacitors (EDLCs). Pseudocapacitors store electrical energy electrochemically, while (EDLCs) store electrical energy electrostatically by reversibly adsorbing and desorbing electrolytic ions at the electrode surface.[30−37] Energy storage in SCs depends upon many factors: (i) the charge separation in EDLC surfaces, where porous carbon

materials are frequently used as electrodes, (ii) the reaction among redox-active organic substituents and electrolytes, and (iii) the reaction takes place at electrode surfaces.[38−40] As a result, the structure and content of the electrode material have a significant impact on SC characteristics.[40−45] Inorganic electrode materials have been widely employed in SCs in recent years, but many have flaws, such as resource scarcity and environmental pollution during the mining process. Many attempts have been undertaken to develop more affordable and eco-friendly electrode materials.[45−50] Organic electrode materials have attracted the interest of many researchers due
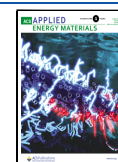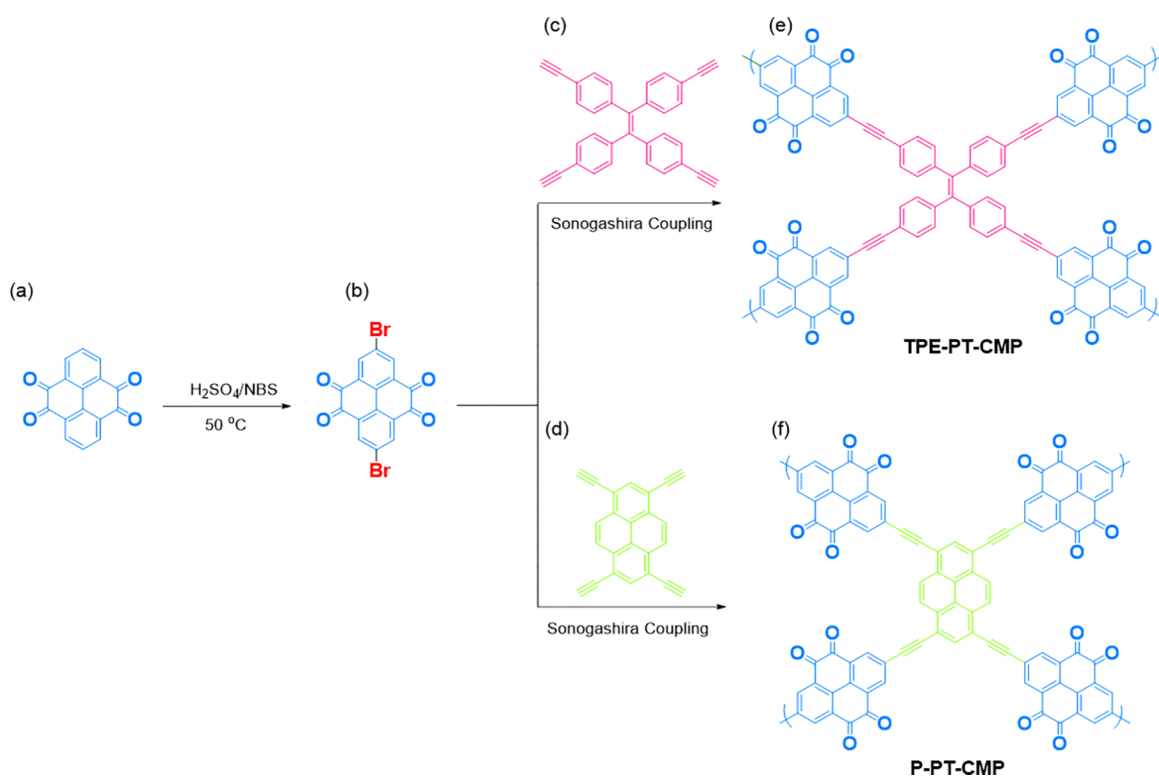
Figure 1. Synthesis of PT-Br$_2$ (b), TPE-PT-CMP (e), and P-PT-CMP (f) from PT (a), TPE-T(c), and Py-T (d).

to their environmentally friendly nature, low energy utilization, flexibility, and significant redox activity.[45−50]

Porous materials are divided into microporous, mesoporous, or macroporous, depending on their pore size. Microporous organic polymers (MOPs) are next-generation materials that are simple to synthesize, have substantial surface areas, excellent thermal stabilities, exceptional pore volumes, and low densities. Specifically, conjugated microporous polymers (CMPs) are one form to prepare MOPs extensively employed in SCs because of their extensive pore structure as essential organic electrode materials.[50−55] CMPs are comprised of a particular π-conjugated structure and a connecting group, with the unique structure unit having redox activity, endowing them with excellent electrochemical performance.[50−55] Besides, CMPs also have porous characteristics, which make them different from other conventional polymers, and thus, CMPs emerge as suitable electrode materials for energy storage applications. So far, many CMPs have been prepared using a variety of chemical and electrochemical processes that connect appropriate building blocks through polymerizations.[55−60]

PT was first designed by Harris et al through a one-pot reaction of pyrene (Py) in the presence of both ruthenium chloride (RuCl$_3$) and sodium periodate (NaIO$_4$).[61] PT contains four carbonyl groups and is also named cyclic 1,2-diketones. The PT material is widely used as redox-active organic electrode materials and displays excellent performance compared to acyclic 1,2-diketone materials due to its active carbonyl sites.[62] Some groups have already designed and constructed COF and POP materials linked to PT for lithium and sodium ions batteries and secondary batteries.[63,64] A pyrene (Py) moiety possesses a planar structure with donor properties and extended π-conjugation.[6,7,22] The preparation of CMPs based on tetraphenylethene (TPE) and pyrene moieties has been used for energy storage, gas capture, dye

removal, and optoelectronic devices.[6,7,22] To the best of our knowledge, this is the first study to construct PT-linked CMPs and investigate these materials in supercapacitors systems. Herein, two CMP samples (TPE-PT-CMP and P-PT-CMP) were prepared using the polycondensation coupling reaction (Sonogashira reaction) based on TPE/Py and PT as building block monomers as shown in Figure 1 for the supercapacitor system. The properties of the resulting two CMPs, including molecular structures, texture and porosity, crystallinity, thermal degradation temperatures, and char yield, were investigated in detail using spectroscopic and microscopic methods such as solid-state Fourier transform infrared (FTIR), nuclear magnetic resonance (NMR), Brunauer, Emmett, and Teller (BET), scanning electron microscopy (SEM), thermal gravimetric analysis (TGA), and transmission electron microscopy (TEM) analyses. The newly obtained two CMPs show moderate surface areas of 120 m^2 g^{-1} for TPE-PT-CMP and 315 m^2 g^{-1} for P-PT-CMP. Due to the presence of a redox-active unit (PT) in these two CMPs, we expected that these two materials would be promising precursors for clean energy storage. The cyclic volumetry (CV) and galvanostatic charge−discharge (GCD) results revealed that both TPE-PT-CMP and P-PT-CMP have high capacitance values and long-term cycling stability compared with other CMPs materials. Our observation proposes that the rational design of PT-linked CMPs could be applied in different multiclean energy applications such as Li, Na, and rechargeable battery applications.

2. EXPERIMENTAL SECTION

2.1. Materials. Ruthenium(III) chloride hydrate (RuCl$_3$·xH$_2$O), triphenylphosphine (PPh$_3$, 99%), pyrene (Py, 98%), N-bromosuccinimide (NBS, 99%), concentrated sulfuric acid (H$_2$SO$_4$), chloroform (CHCl$_3$), methanol (MeOH), triethylamine (Et$_3$N), dimethylformamide (DMF), tetrahydrofuran (THF), Pd(PPh$_3$)$_4$, sodium periodate
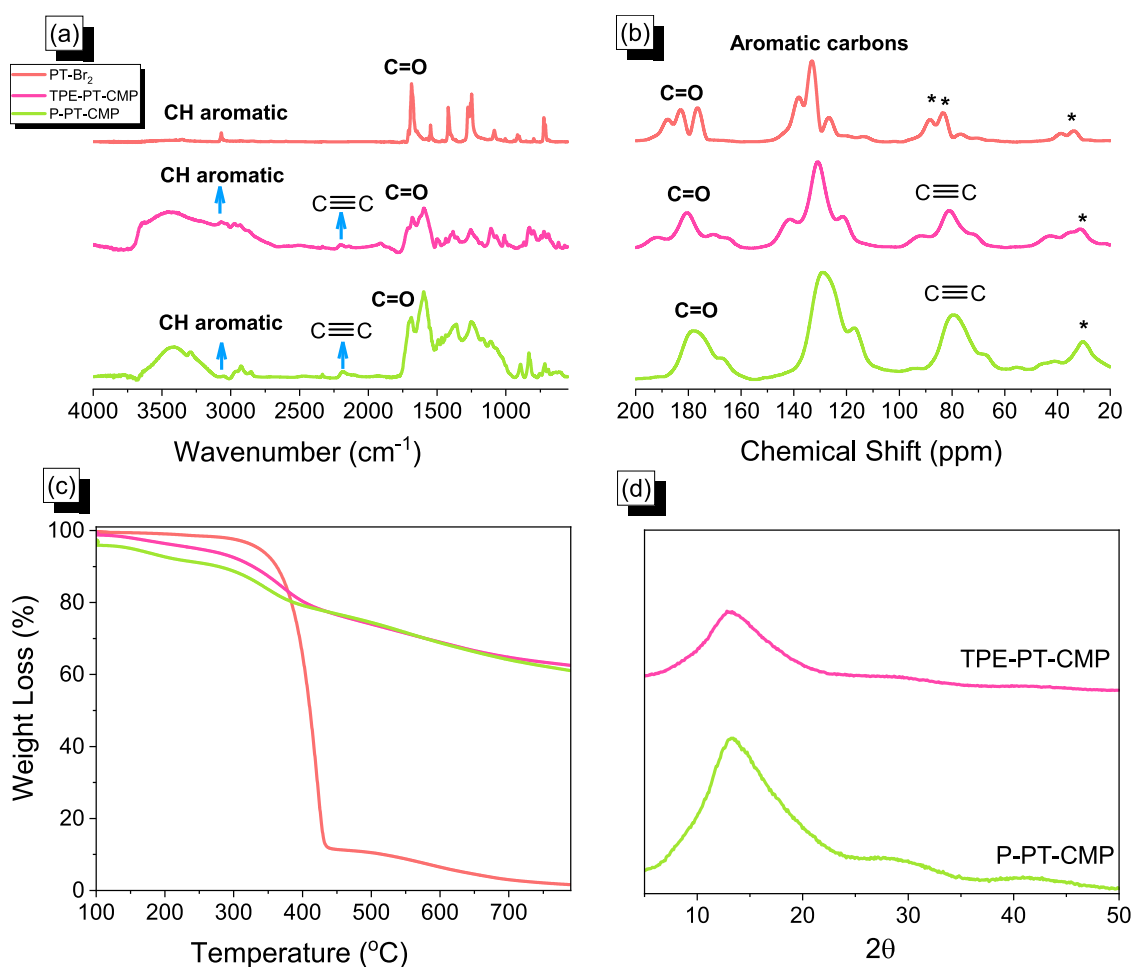
Figure 2. FTIR (a), solid-state ^{13}C NMR (b), TGA (c), and XRD (d) analyses of PT-Br$_2$, TPE-PT-CMP, and P-PT-CMP.

(NaIO$_4$, 99.8%), and copper iodide (CuI, 98%) were bought from Sigma-Aldrich. The Py-T and TPE-T monomers used in this study were obtained using our reported procedures [Schemes S1 and S2 and Figures S1−S6].[65,66]

2.2. Synthesis of PT. Sodium periodate (211 mM, 45.0 g), acetonitrile (103 mL), dichloromethane (DCM) (103 mL), H$_2$O (129 mL), Py (25.70 mM, 5.14 g), and RuCl$_3$·xH$_2$O (0.54 mM, 0.64 g) were charged in a dried round flask (500 mL). The solution mixture was stirred and kept at 40 °C for 24 h, and the obtained suspension was washed several times with DCM. The yellow powder was obtained after removing DCM under reduced pressure, and the solid was recrystallized using CHCl$_3$ (1.54 g, 23%, Figure 1). FTIR (cm^{-1}, Figure S7): 3060, 1675 (C=O), 1562, 1418, 1346, 1278, 1057, 913. ^{1}H NMR (500 MHz, DMSO-d_6, δ, ppm, Figure S8): 8.32 (4H), 7.74 (2H). ^{13}C NMR (125 MHz, DMSO-d_6, δ, ppm, Figure S9): 178.43 (C=O), 134.88, 132.51, 130.92. HR-FD-MS: m/z: 263.032 (Figure S10).

2.3. Synthesis of PT-Br$_2$. PT (1.20 g, 4.56 mmol) was added to a cooled Schlenk flask, and then, 30 mL of concentrated H$_2$SO$_4$ and NBS (1.80 g, 10.20 mmol) was added to the flask, and the obtained solution was heated for 5 h at 50 °C. The resulting yellow powder was purified by the recrystallization in DMSO and washed with DCM and ether to afford PT-Br$_2$ as a yellow solid (1.26 g, 68%, Figure 1). FTIR (cm^{-1}, Figure S11): 3070, 1679 (C=O), 1545, 1421, 1260. ^{1}H NMR (DMSO-d_6, 500 MHz, Figure S12): δ = 8.36 (4H). ^{13}C NMR data of PT-Br$_2$ is not provided due to its poor solubility. HR-FD-MS: m/z: 421.328 (Figure S13). PT-Br$_2$ had crystalline properties according to X-ray diffraction (XRD) analysis (Figure S14).

2.4. Preparation of TPE-PT-CMP and P-PT-CMP. PPh$_3$ (0.03 mmol), CuI (0.03 mmol), Pd (0.03 mmol), PT-Br$_2$ (0.50 mmol), TPE-T (0.25 mmol) or Py-T (0.25 mmol), 5 mL of Et$_3$N, and 5 mL

of DMF were charged in a dried Schlenk flask (25 mL) and stirred for 30 min at room temperature under a N$_2$ atmosphere. Then, the solution was refluxed at 115 °C for 72 h. The obtained black solid was immersed for 1 h in MeOH, THF, and acetone and then dried at 110 °C for 8 h to afford TPE-PT-CMP (yield: 87%) or P-PT-CMP as a black powder (yield: 83%, Figure 1).

3. RESULTS AND DISCUSSION

3.1. Synthesis and Characterization of TPE-PT and P-PT-CMPs. In this work, we designed and constructed TPE-PT-

Table 1. Obtained TGA, BET, and Capacitance Data of TPE-PT-CMP and P-PT-CMP

sample	T_{d10} (°C)	char yield (wt %)	surface area (m^2 g^{-1})	pore volume (cm^3 g^{-1})	pore size (nm)	capacity at 0.5 A g^{-1} (F g^{-1})
TPE-PT-CMP	328	63	120	0.05	2.1−3.98	242
P-PT-CMP	227	61	315	0.33	1.1−3.02	440

CMP and P-PT-CMP containing pyrene-4,5,9,10-tetraone (PT) with four C=O groups as the active sites through a rapid and efficient Sonogashira−Hagihara coupling reaction. PT was synthesized through the reaction between pyrene with RuCl$_3$·xH$_2$O as the catalyst in the presence of NaIO$_4$ as the oxidant to afford a yellow solid with a yield of up to 23% as
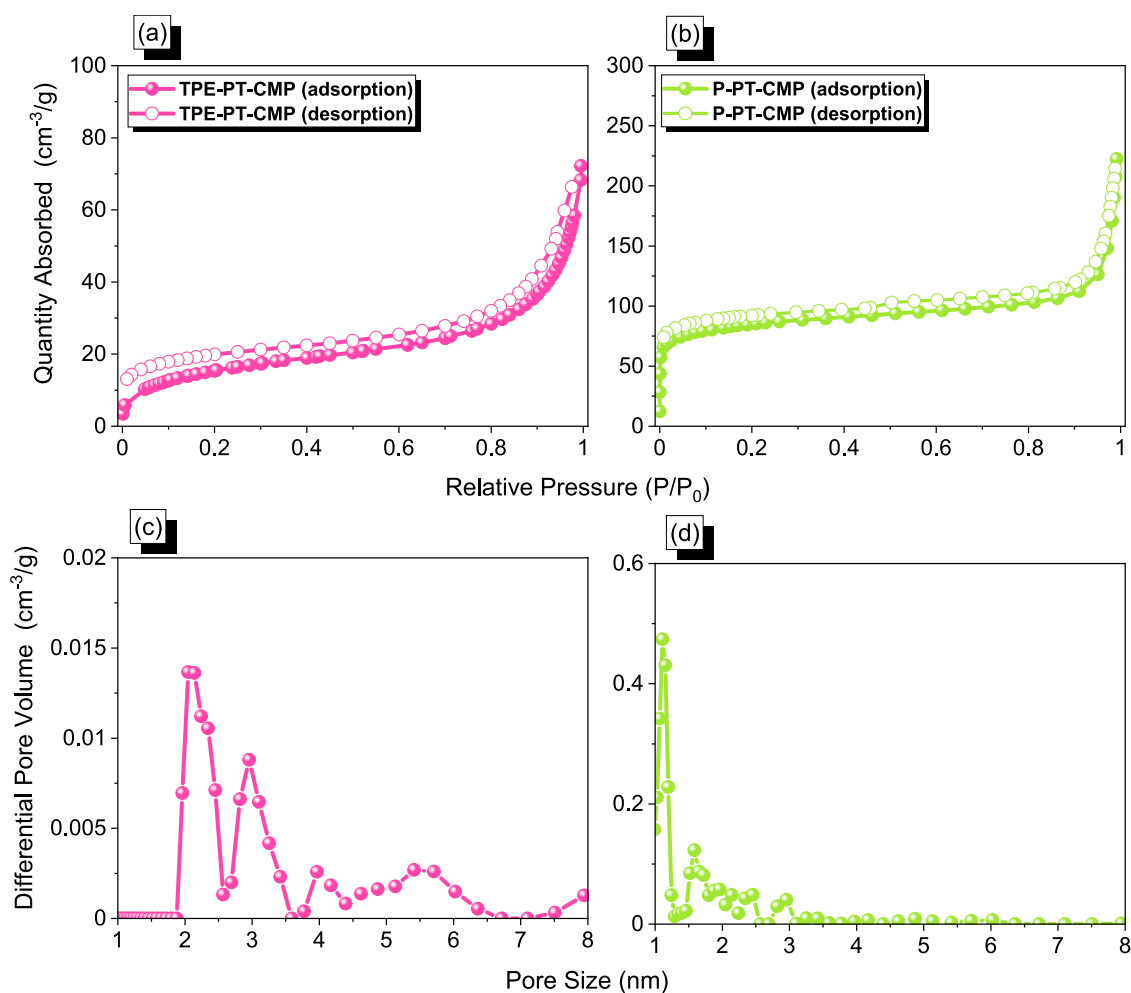
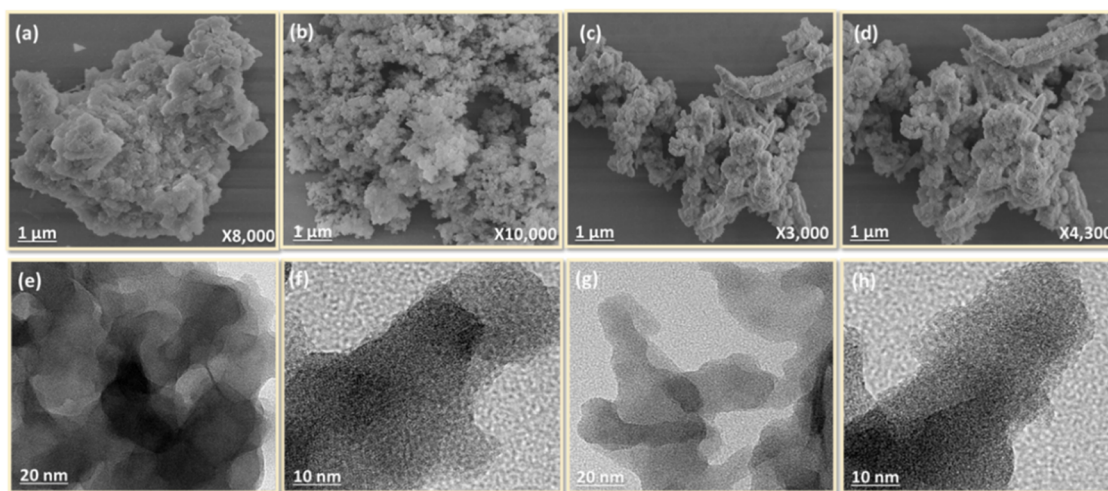**Figure 3.** N_2 sorption and PSD curves of TPE-PT-CMP (a, c) and P-PT-CMP (b, d).

Figure 4. SEM and TEM images of TPE-PT-CMP (a, b, e, f) and P-PT-CMP (c, d, g, h).

presented in Figure 1a. Then, $PT-Br_2$ was obtained with high purity and yield via the reaction of PT with NBS in the presence of concentrated H_2SO_4 at 50 °C [Figure 1b]. We used the Sonogashira coupling reaction to prepare TPE-PT-CMP and P-PT-CMP as a black powder through the reaction of TPE-T and Py-T [Figure 1c,d], respectively, with $PT-Br_2$ in a mixture of Et_3N/DMF and $Pd(PPh_3)_4$ at 110 °C for 72 h

[Figure 1c,d]. We observed that the solubility of TPE-PT-CMP and P-PT-CMP is poor in all organic solvents, such as DMF, THF, NMP, MeOH, and acetone, indicating that both materials exhibited superior cross-linked networks, which are attributed to a high degree of polymerization. The obtained PT and $PT-Br_2$ monomers were analyzed using FTIR and NMR
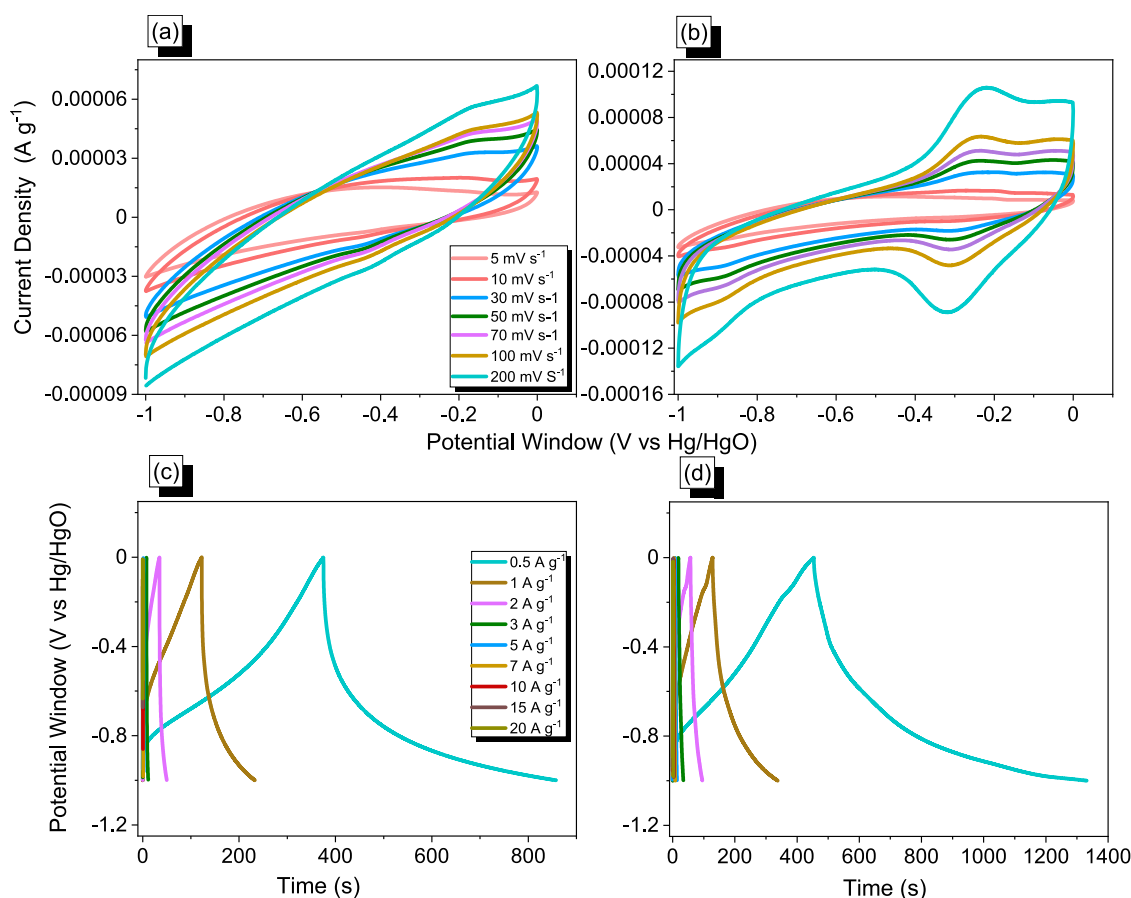
Figure 5. CV and GCD analyses of TPE-PT-CMP (a, c) and P-PT-CMP (b, d).

measurements, and all data are presented in the Supporting Information [Figures S7−S13].

The chemical structure, thermal stability, and crystalline properties of TPE-PT-CMP and P-PT-CMP were carefully characterized using solid-state ^{13}C nuclear magnetic resonance (NMR), FTIR spectroscopy, TGA, and powder X-ray diffraction (XRD), as outlined in Figure 2. For more details, the FTIR spectra of PT-Br$_2$ and PT-CMPs at 25 °C are presented in Figure 2a, which shows that the absorption bands located in the region of 3062−3057 and 1696−1687 cm^{-1} for all PT-Br$_2$ and PT-CMPs refer to the presence of C−H stretching in the aromatic ring and C=O units in the PT structure. In addition, the peaks were observed at 3462 and 2196 cm^{-1} for TPE-PT-CMP and 3427 and 2187 cm^{-1} for P-PT-CMP, referring to the water adsorbed and terminal alkynyl group, respectively, in these two materials. More details about the chemical structures of TPE-PT-CMP and P-PT-CMP were examined using solid-state ^{13}C NMR as presented in Figure 2b. Figure 2b shows the carbon resonance signals centered at 180 ppm and in the range from 138 to 127 pm for PT-Br$_2$, TPE-PT-CMP, and P-PT-CMP, which are assigned to carbonyl groups and aromatic rings. In addition, the presence of signals at 81.30 and 79.87 ppm corresponds to the carbon nucleus for internal and alkynyl groups, respectively, in their framework. As expected, TPE-PT-CMP and P-PT-CMP displayed good thermal stability after the attachment of the PT unit through the Sonogashira coupling reaction [Figure 2c and Table 1]. For example, the degradation temperature at 10 wt % and the char yield were 328 °C and 63 wt % for TPE-PT-CMP and 227 °C and 61 wt % for P-PT-CMP. Furthermore, the XRD patterns

[Figure 2d] of all synthesized samples did not show any obvious peaks indicating their amorphous structures.

We assessed N$_2$ adsorption and desorption analyses to investigate the porosity properties of TPE-PT-CMP and P-PT-CMP, recorded at 77 K [Figure 3].

The adsorption−desorption profiles of both TPE-PT-CMP and P-PT-CMP manifested type I and IV characteristics [Figure 3a,b]. The fast N$_2$ uptake in the low-pressure range for both CMP samples pronounced that TPE-PT-CMP and P-PT-CMP are microporous materials. Then, at relative pressures ranging (P/P_0) from 0.1 to 0.8, the N$_2$ adsorption increased. Furthermore, both N$_2$ isotherms displayed constant nitrogen uptakes when P/P_0 was up to 0.8, which suggests the coexistence of both mesopores and macropores in the two CMPs networks. The BET surface area and total pore volume were determined to be 120 m^2 g^{-1} and 0.05 cm^3 g^{-1} for TPE-PT-CMP and 315 m^2 g^{-1} and 0.33 cm^3 g^{-1} for P-PT-CMP, respectively. Furthermore, the pore size distributions of TPE-PT and P-PT-CMPs were measured using nonlocal density functional theory (NLDFT) [Figure 3c,d]. The TPE-PT-CMP has the main peak located at 2.1 nm and other peaks in the range of 2.92−5.60 nm. In addition, the P-PT-CMP rejoiced peaks in the range of 1.10−3.02 nm. The TPE-PT-CMP and P-PT-CMP frameworks contain microporous and mesoporous structures according to their pore size [Figure 3c,d].

The morphologies of the prepared PT-CMPs were studied by employing both high-resolution SEM and TEM techniques [Figure 4]. The SEM images of TPE-PT-CMP elucidated an aggregated spherical shape and P-PT-CMP displayed an aggregated rod-like structure. In addition, the TEM images
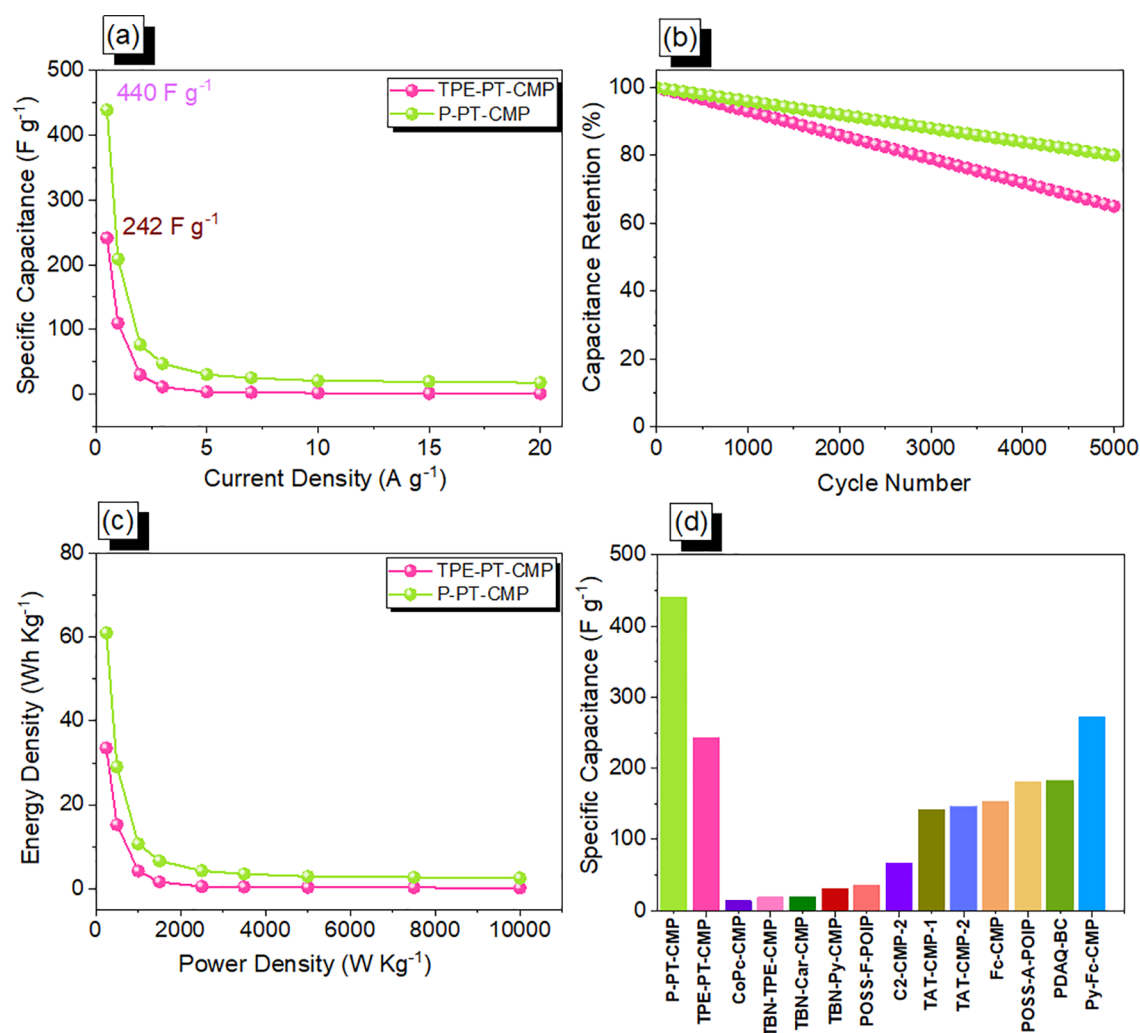
Figure 6. Capacitance (a), capacitance retention (b), Ragone curves (c) of TPE-PT-CMP and P-PT-CMP, and (d) Comparison of specific capacitances of the TPE-PT-CMP and P-PT-CMP materials with other CMPs previously studied for energy storage applications.

showed fused and aggregated particle-like shape morphologies for prepared TPE-PT and P-PT-CMPs.

3.2. Electrochemical Performance of TPE-PT-CMP and P-PT-CMP. In a 1.0 M KOH aqueous solution, the electrochemical performances of both the CMPs were evaluated using cyclic voltammetry (CV) and galvanostatic charge−discharge (GCD) profiles with a three-electrode system consisting of glassy carbon, Hg/HgO, and platinum wire as the working, reference, and counter electrodes, respectively. The CV curves of TPE-PT-CMP and P-PT-CMP are shown in Figure 5a,b, for a wide range of scan speeds from 5 to 200 mV s^{-1}, with a possible potential window between −1.0 and 0.0 V (versus Hg/HgO). It is clear that the characteristic quasi-rectangle-like humped shape was achieved for all of the CMPs that were harmonious with various scan ranges, demonstrating that the acquired CMPs are steady in terms of current sweep and depict capacitance from EDLC.[6,35,67−70] Both EDLC and redox reactions contribute to supercapacitor storage qualities.[6,35] In the case of the CV of P-PT-CMP, we can plainly detect two notable redox peaks, an oxidation peak at −0.25 V, and a reduction peak at −0.21 V versus Hg/HgO, showing that redox processes play a significant role.[67−70] The distinct contrast in a CV shape between TPE-PT-CMP and P-PT-CMP demonstrates that the

total capacitance in P-PT-CMP is dispersed throughout the whole voltage range, emphasizing the relevance of surface area and narrow pore dispersion over TPE-PT-CMP. The CV curves show that, as the scan rises, the specific capacitance drops because the oxidation−reduction process does not react completely in time at higher scan rates.[67−70] Furthermore, the charge/discharge profile and capacitance of these compounds were tested from 0.5 to 20 A g^{-1} current densities [Figure 5a,b]. These GCD curves exhibited a triangular, tiny bend in the shape, showing both pseudo-capacity and EDLC properties.[67−70] The charging time of both the CMPs is shorter than that of the discharging time, indicating better capacitance.[68−70] The discharge time of P-PT-CMP is more than that of TPE-PT-CMP, indicating higher specific capacitance and consistency with the obtained CV curves.[69,70]

Further, the ions in the electrolyte have ample time to reach all of the active sites of the electroactive materials at low scan ratesl; hence, an increase in the capacitance is observed. On the other hand, at higher scan rates, the electrolyte reaches the electroactive materials in a shorter amount of time, resulting in decreased capacitance, which is evident in the GCD profiles.[6,35,70] The specific capacitance of P-PT-CMP and TPE-PT-CMP at 0.5 A g^{-1} was 440 and 242 F g^{-1}, calculated using eq S1 in the supporting information [Figure 6a]. With
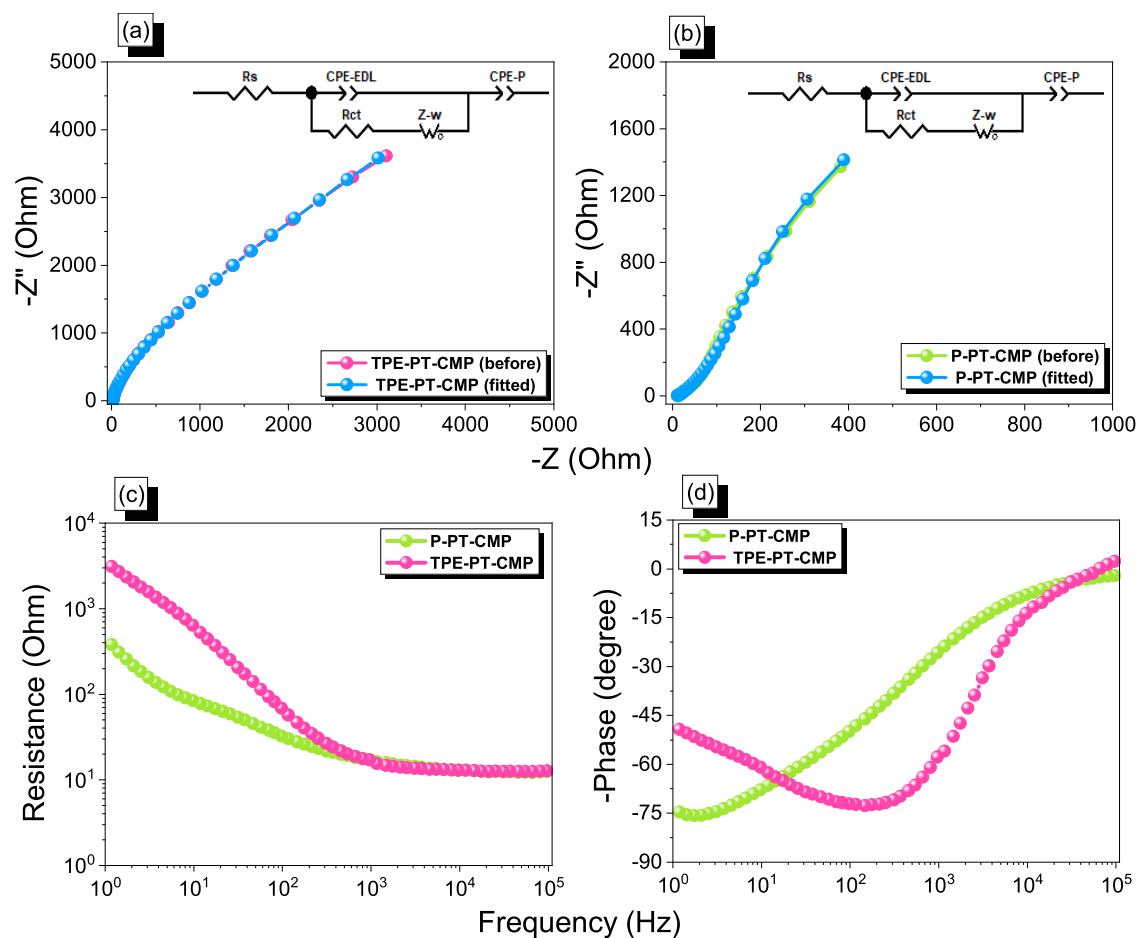
Figure 7. (a, b) Nyquist plots with equivalent fitted circuit, (c) Bode plots of the frequency-dependent magnitude, and (d) the frequency-dependent phase angle of the TPE-PT-CMP and P-PT-CMP materials.

the increase in current density, the specific capacitance of P-PT-CMP remains higher than TPE-PT-CMP. This trend can be explained using the chemistry and surface areas of the parent molecules. The pyrene moiety in P-PT-CMP consists of fused benzene rings leading to strong $\pi-\pi$ interaction and consistent electron conductivity helping to form pores for transportation of electrolyte ions. In addition, the higher surface area of P-PT-CMP facilitates this. We observed that the specific capacitance of P-PT-CMP and TPE-PT-CMP decreased gradually with increasing current density because the electrolyte ions do not have enough time to migrate through pores and only the exterior active surface is used for charge storage at higher current density.

Furthermore, Figure 6b shows that our TPE-PT-CMP and P-PT-CMP feature long-term cycling stability with capacitance retentions of 65, and 85%, respectively, over 5000 cycles at a 10 A g^{-1}. We used eqs S2 and S3 [see supporting information] to calculate the energy and power densities and construct a Ragone plot of TPE-PT-CMP and P-PT-CMP [Figure 6c]. The calculated energy density was found to be 33.2 and 61 W h kg^{-1}, respectively, for TPE-PT-CMP and P-PT-CMP. Figure 6d shows that both precursors (TPE-PT-CMP and P-PT-CMP) have outstanding supercapacitor performance compared with other CMP materials at the same current density (0.5 A g^{-1}). Subsequently, EIS was employed to understand the ion diffusion mechanism and the resistance offered by the electrodes. The Nyquist plot has been presented in Figure 7a,b, along with its equivalent fitted circuit to study charge transfer resistance and series resistance.

The analogous series resistance, charge transfer resistance, constant phase elements representing EDLC and pseudocapacitive behavior, and Warburg element, respectively, are represented by Rs, Rct, CPE−EDL, CPE−P, and Zw in the fitting circuit. The ohmic resistances of P-PT-CMP and TPE-PT-CMP are 11.81 and 12.17 Ω, respectively, while the charge transfer resistance of P-PT-CMP and TPE-PT-CMP are 3336 and 900 Ω, respectively [Table S1]. Aside from that, Figure 7c depicts a Bode plot showing the frequency-dependent magnitude. The results show sloping lines with a negative slope at low frequencies and minimal resistance at high frequencies, confirming the electrode materials' outstanding capacitive properties. Figure 7d shows electrodes' frequency-dependent phase angle plots. At a phase angle of −45°, the knee frequencies were studied when the capacitive and resistive characteristics of electrodes were equal. The knee frequencies of P-PT-CMP and TPE-PT-CMP are 161.58 and 2036.47 Hz, respectively. It is already a published fact that the knee frequency values are indicative of the rate capability of the compounds, and they are proportionally related. Hence, according to the data above, both P-PT-CMP and TPE-PT-CMP are better electrode materials due to their superior rate performance, which is consistent with the specific capacitance curve (Figure 6a).

Furthermore, we have evaluated the electrochemical performance of a symmetric supercapacitor using a CR2032

coin cell made up of a bottom and up cover, metal spring, separator, anode and cathode, and electrolyte. We used our PT-CMPs as cathode and anode to construct a symmetric supercapacitor device. The slurry was prepared as per the ratio mentioned in the paper and cast on carbon paper [see Supporting Information]. We used Selemion AMV membrane for an aqueous 1.0 M KOH electrolyte. All electrochemical measurements were carried out within a potential range of -1.0 to 0 V at different scan rates from $5-200$ mV s^{-1} as well as different current densities from 0.5 to 7 A g^{-1} for CV and GCD analysis, respectively. The electrochemical characterization was performed in 1M KOH at potentials ranging from -1 to 0 V. Cyclic voltammetry profiles were acquired at various scan speeds ranging from $5-200$ mV s^{-1}, and galvanostatic charge−discharge curves were recorded at various current densities ranging from 0.5 to 7 A g^{-1}. Figure S15a and b illustrates the CV curves at different scan speeds ranging from $5-200$ mV s^{-1}, respectively. All of the compound's cyclic voltammograms displayed almost rectangular forms with humps, which are hallmarks of a supercapacitor. Even at greater scan rates, electrode integrity was preserved because higher scan rates resulted in higher current density, showing superior kinetics and rate capacity. The GCD curves [Figure S15c and d] of TPE-PT-CMP and P-PT-CMP were measured at a current density between $0.5-7$ A g^{-1}. The results indicate the almost triangular shape for all of the CMPs with the presence of little bent during charge, suggesting the combined effect of pseudocapacitive and EDLC. In addition, the discharging time was higher than the charging time, indicating the improved performance of all of the CMPs for practical applications. The specific capacitance values of P-PT-CMP and TPE-PT-CMP at 0.5 A g^{-1} were 286 and 57 F g^{-1}; respectively. In addition, Figure S16 shows that both TPE-PT-CMP and P-PT-CMP in symmetric supercapacitor devices featured long-term cycling stability with capacitance retentions of 85 and 99%, respectively, over 5000 cycles at a current density of 5 A g^{-1}. The glowing LED photograph with the P-PT-CMP symmetric coin supercapacitor is shown in Figure S17.

4. CONCLUSIONS

To conclude, we used the Sonogashira polycondensation reaction to construct two types of PT-CMPs containing PT units through the reaction of a brominated PT (PT-Br$_2$) as a building block with ethynyl derivatives of TPE and Py molecules for energy storage applications as organic electrode precursors. The data demonstrated that the prepared P-PT-CMP featured high BET surface areas (315 m^2 g^{-1}), total pore volume (0.33 cm^3 g^{-1}), pore size in the range 1.1−3.02 nm, char yield up to 60 wt %, and rod-like morphologies. The electrochemical results of P-PT-CMP show high cycling stability of up to 80% and specific capacitance of 440 F g^{-1} due to its interesting suitable porosity properties, presence of PT moiety, and rod morphologies. When used as candidates for electrode materials, these porous molecules have also delivered outstanding performances when employed as a symmetric coin cell for supercapacitors. Thus, because of comprehensive advantages, including good specific capacitance, facile synthesis method, suitable surface area, and tunable morphologies of PT-linked CMPs, we believe that both newly obtained CMPs materials are excellent candidates for energy storage. These materials can open doors for other potential applications in clean energy such as rechargeable batteries, Li-ion positive electrodes, and sodium and lithium-ion batteries.

■ ASSOCIATED CONTENT

ⓈI Supporting Information

The Supporting Information is available free of charge at https://pubs.acs.org/doi/10.1021/acsaem.2c01842.

Details about characterization methods and electrochemical analysis; values of different parameters of fitted Nyquist plots data of TPE-PT-CMP and P-PT-CMP; synthesis of Py-TMS and Py-T; synthesis of TPE-TMS and TPE-T; FTIR spectrum of Py-T; ^{1}H NMR spectrum of Py-T; ^{13}C NMR spectrum of Py-T; FTIR spectrum of TPE-T; ^{1}H NMR spectrum of TPE-T; ^{13}C NMR spectrum of TPE-T; FTIR profile of PT; ^{1}H NMR profile of PT; ^{13}C NMR profile of PT; high-resolution FD-MS spectrum of PT; FTIR profile of PT-Br$_2$; ^{1}H NMR profile of PT-Br$_2$; high-resolution FD-MS spectrum of PT-Br$_2$; XRD spectrum of PT-Br$_2$, CV, and GCD analyses of TPE-PT-CMP and P-PT-CMP as organic electrodes in symmetric coin supercapacitors; cycling stability performance of TPE-PT-CMP and P-PT-CMP measured at a current density of 5 A g^{-1} for 5000 cycles; and glowing LED photograph with a P-PT-CMP symmetric coin supercapacitor (PDF)

■ AUTHOR INFORMATION

Corresponding Authors

Mohamed Gamal Mohamed − *Department of Materials and Optoelectronic Science and College of Semiconductor and Advanced Technology Research, National Sun Yat-Sen University, Kaohsiung 804, Taiwan; Chemistry Department, Faculty of Science, Assiut University, Assiut 71515, Egypt;* ⓘ orcid.org/0000-0003-0301-8372; Email: mgamal.eldin12@yahoo.com

Shiao-Wei Kuo − *Department of Materials and Optoelectronic Science and College of Semiconductor and Advanced Technology Research, National Sun Yat-Sen University, Kaohsiung 804, Taiwan; Department of Medicinal and Applied Chemistry, Kaohsiung Medical University, Kaohsiung 807, Taiwan;* ⓘ orcid.org/0000-0002-4306-7171; Email: kuosw@faculty.nsysu.edu.tw

Authors

Swetha V. Chaganti − *International PhD Program for Science, National Sun Yat-sen University, Kaohsiung 80424, Taiwan; Department of Chemistry, National Sun Yat-Sen University, Kaohsiung 80424, Taiwan*

Santosh U. Sharma − *International PhD Program for Science, National Sun Yat-sen University, Kaohsiung 80424, Taiwan; Department of Chemistry, National Sun Yat-Sen University, Kaohsiung 80424, Taiwan*

Maha Mohamed Samy − *Department of Materials and Optoelectronic Science and College of Semiconductor and Advanced Technology Research, National Sun Yat-Sen University, Kaohsiung 804, Taiwan; Chemistry Department, Faculty of Science, Assiut University, Assiut 71515, Egypt*

Mohsin Ejaz − *Department of Materials and Optoelectronic Science and College of Semiconductor and Advanced Technology Research, National Sun Yat-Sen University, Kaohsiung 804, Taiwan*

Jyh-Tsung Lee − *International PhD Program for Science, National Sun Yat-sen University, Kaohsiung 80424, Taiwan; Department of Chemistry, National Sun Yat-Sen University, Kaohsiung 80424, Taiwan; Department of Medicinal and Applied Chemistry, Kaohsiung Medical University, Kaohsiung 807, Taiwan;* orcid.org/0000-0002-2658-4222

Kan Zhang − *Research School of Polymeric Materials, School of Materials Science and Engineering, Jiangsu University, Zhenjiang 212013, China;* orcid.org/0000-0003-4628-2704

Complete contact information is available at:
https://pubs.acs.org/10.1021/acsaem.2c01842

Notes
The authors declare no competing financial interest.

■ REFERENCES

(1) Tan, Y.; Xu, C.; Chen, G.; Liu, Z.; Ma, M.; Xie, Q.; Zheng, N.; Yao, S. Synthesis of Ultrathin Nitrogen-Doped Graphitic Carbon Nanocages as Advanced Electrode Materials for Supercapacitor. *ACS Appl. Mater. Interfaces* **2013**, *5*, 2241−2248.

(2) Samy, M. M.; Mohamed, M. G.; Kuo, S. W. Directly synthesized nitrogen-and-oxygen−doped microporous carbons derived from a bio-derived polybenzoxazine exhibiting high-performance super-capacitance and CO_2 uptake. *Eur. Polym. J.* **2020**, *138*, No. 109954.

(3) Shi, R.; Han, C.; Duan, H.; Xu, L.; Zhou, D.; Li, H.; Li, J.; Kang, F.; Li, B.; Wang, G. Redox-Active Organic Sodium Anthraquinone-2-Sulfonate (AQS) Anchored on Reduced Graphene Oxide for High-Performance Supercapacitors. *Adv. Energy Mater.* **2018**, *8*, No. 1802088.

(4) Mohamed, M. G.; Atayde, E. C., Jr; Matsagar, M. B.; Na, J.; Yamauchi, Y.; Wu, K. C. W.; Kuo, S. W. Construction Hierarchically Mesoporous/Microporous Materials Based on Block Copolymer and Covalent Organic Framework. *J. Taiwan Inst. Chem. Eng.* **2020**, *112*, 180−192.

(5) Mohamed, M. G.; Mansoure, T. H.; Takashi, Y.; Samy, M. M.; Chen, T.; Kuo, S. W. Ultrastable porous organic/inorganic polymers based on polyhedral oligomeric silsesquioxane (POSS) hybrids exhibiting high performance for thermal property and energy storage. *Microporous Mesoporous Mater.* **2021**, *328*, No. 111505.

(6) Samy, M. M.; Mohamed, M. G.; Kuo, S. W. Pyrene-functionalized tetraphenylethylene polybenzoxazine for dispersing single-walled carbon nanotubes and energy storage. *Compos. Sci. Technol.* **2020**, *199*, No. 108360.

(7) Mohamed, M. G.; Chaganti, S. V.; Li, M. S.; Samy, M. M.; Sharma, S. U.; Lee, J. T.; Elsayed, M. H.; Chou, H. H.; Kuo, S. W. Ultrastable Porous Organic Polymers Containing Thianthrene and Pyrene Units as Organic Electrode Materials for Supercapacitors. *ACS Appl. Energy Mater.* **2022**, *5*, 6442−6452.

(8) Liu, S.; Kang, L.; Henzie, J.; Zhang, J.; Ha, J.; Amin, M. A.; Hossain, M. S. A.; Jun, S. C.; Yamauchi, Y. Recent Advances and Perspectives of Battery-Type Anode Materials for Potassium Ion Storage. *ACS Nano* **2021**, *15*, 18931−18973.

(9) Abuzeid, H. R.; EL-Mahdy, A. F. M.; Kuo, S. W. Covalent organic frameworks: Design principles, synthetic strategies, and diverse applications. *Giant* **2021**, *6*, No. 100054.

(10) Liu, S.; Kang, L.; Hu, J.; Jung, E.; Zhang, J.; Jun, S. C.; Yamauchi, Y. Unlocking the Potential of Oxygen-Deficient Copper-Doped Co_3O_4 Nanocrystals Confined in Carbon as an Advanced Electrode for Flexible Solid-State Supercapacitors. *ACS Energy Lett.* **2021**, *6*, 3011−3019.

(11) Liu, S.; Kang, L.; Zhang, J.; Jung, E.; Lee, S.; Jun, S. C. Structural engineering and surface modification of MOF-derived cobalt-based hybrid nanosheets for flexible solid-state supercapacitors. *Energy Storage Mater.* **2020**, *32*, 167−177.

(12) Samy, M. M.; Mekhemer, I. M. A.; Mohamed, M. G.; Elsayed, M. H.; Lin, K. H.; Chen, Y. K.; Wu, T. L.; Chou, H. H.; Kuo, S. W. Conjugated microporous polymers incorporating Thiazolo[5,4-d]-thiazole moieties for Sunlight-Driven hydrogen production from water. *Chem. Eng. J.* **2022**, *446*, No. 137158.

(13) Amin, K.; Ashraf, N.; Mao, L.; Faul, C. F. J.; Wei, Z. Conjugated microporous polymers for energy storage: Recent progress and challenges. *Nano Energy* **2021**, *85*, No. 105958.

(14) Mei, L.; Wei, J.-C.; Duan, Q. Construction of copper porphyrinlinked conjugated microporous polymer/carbon nanotube composite as flexible electrodes for supercapacitors. *J. Mater. Sci.: Mater. Electron.* **2021**, *32*, 24953−24963.

(15) Zhang, C.; He, Y.; Mu, P.; Wang, X.; He, Q.; Chen, Y.; Zeng, J.; Wang, F.; Xu, Y.; Jiang, J.-X. Toward High Performance Thiophene Containing Conjugated Microporous Polymer Anodes for Lithium-Ion Batteries through Structure Design. *Adv. Funct. Mater.* **2018**, *28*, No. 1705432.

(16) Li, L.; Lu, F.; Xue, R.; Ma, B. L.; Li, Q.; Wu, N.; Liu, H.; Yao, W. Q.; Guo, H.; Yang, W. Ultrastable triazine-based covalent organic framework with an interlayer hydrogen bonding for supercapacitor applications. *ACS Appl Mater Interfaces* **2019**, *11*, 26355−26363.

(17) Weng, Z.; Su, Y.; Wang, D. W.; Li, F.; Du, J.; Cheng, H. M. Graphene−cellulose paper flexible supercapacitors. *Adv. Energy Mater.* **2011**, *1*, 917−922.

(18) Mohamed, M. G.; EL-Mahdy, A. F. M.; Kotp, M. G.; Kuo, S. W. Advances in porous organic polymers: syntheses, structures, and diverse applications. *Mater. Adv.* **2022**, *3*, 707−733.

(19) Xu, Z.; Sun, S.; Han, Y.; Wei, Z.; Cheng, Y.; Yin, S.; Cui, W. High-Energy-Density Asymmetric Supercapacitor Based on a Durable and Stable Manganese Molybdate Nanostructure Electrode for Energy Storage Systems. *Appl. Energy Mater.* **2020**, *3*, 5393−5404.

(20) Young, C.; Park, T.; Yi, J. W.; Kim, J.; Hossain, M. S. A.; Kaneti, Y. V.; Yamauchi, Y. Advanced Functional Carbons and Their Hybrid Nanoarchitectures Towards Supercapacitor Applications. *ChemSusChem* **2018**, *11*, 3546−3558.

(21) Najib, S.; Erdem, E. Current progress achieved in novel materials for supercapacitor electrodes: mini review. *Nanoscale Adv.* **2019**, *1*, 2817−2827.

(22) Mohamed, M. G.; Ahmed, M. M. M.; Du, W.-T.; Kuo, S.-W. Meso/Microporous Carbons from Conjugated Hyper-Crosslinked Polymers Based on Tetraphenylethene for High-Performance CO_2 Capture and Supercapacitor. *Molecules* **2021**, *26*, 738.

(23) Samy, M. M.; Sharma, S. U.; Mohamed, M. G.; Mohammed, A. A. K.; Chaganti, S. V.; Lee, J. T.; Kuo, S. W. conjugated microporous polymers containing ferrocene units for high carbon dioxide uptake and energy storage. *Mater. Chem. Phys.* **2022**, *287*, No. 126177.

(24) Kim, D.; Kang, J.; Yan, B.; Seong, K.-d.; Piao, Y. Ambient Temperature Synthesis of Iron-Doped Porous Nickel Pyrophosphate Nanoparticles with Long-Term Chemical Stability for High-Performance Oxygen Evolution Reaction Catalysis and Supercapacitors. *ACS Sustainable Chem. Eng.* **2020**, *8*, 2843−2853.

(25) Wulan Septiani, N. L.; Kaneti, Y. V.; Fathoni, K. B.; Wang, J.; Ide, Y.; Yuliarto, B.; Nugraha, B.; Dipojono, H. K.; Nanjundan, A. K.; Golberg, D.; Bando, Y.; Yamauchi, Y. Self-Assembly of Nickel Phosphate-Based Nanotubes into Two-Dimensional Crumpled Sheet-Like Architectures for High-Performance Asymmetric Supercapacitors. *Nano Energy* **2020**, *67*, No. 104270.

(26) Wang, F.; Wu, X.; Yuan, X.; Liu, Z.; Zhang, Y.; Fu, L.; Zhu, Y.; Zhou, Q.; Wu, Y.; Huang, W. Latest advances in supercapacitors: from new electrode materials to novel device designs. *Chem. Soc. Rev.* **2017**, *46*, 6816−6854.

(27) Mohamed, M. G.; Samy, M. M.; Mansoure, T. H.; Li, C. J.; Li, W. C.; Chen, J. H.; Zhang, K.; Kuo, S. W. Microporous Carbon and

Carbon/Metal Composite Materials Derived from Bio-Benzoxazine-Linked Precursor for CO$_2$ Capture and Energy Storage Applications. *Int. J. Mol. Sci.* **2022**, *23*, No. 347.

(28) Khattak, A. M.; Sin, H.; Ghazi, Z. A.; He, X.; Liang, B.; Khan, N. A.; Alanagh, H. R.; Iqbal, A.; Li, L. S.; Tang, Z. T. Controllable fabrication of redox-active conjugated microporous polymer on reduced graphene oxide for high performance faradaic energy storage. *J. Mater. Chem. A* **2018**, *6*, 18827−18832.

(29) Béguin, F.; Presser, V.; Balducci, A.; Frackowiak, E. Carbons and electrolytes for advanced supercapacitors. *Adv. Mater.* **2014**, *26*, 2219−2251.

(30) Samy, M. M.; Mohamed, M. G.; Mansoure, T. H.; Meng, T. S.; Khan, M. A. R.; Liaw, C. C.; Kuo, S. W. Solid state chemical transformations through ring-opening polymerization of ferrocene-based conjugated microporous polymers in host−guest complexes with benzoxazine-linked cyclodextrin. *J. Taiwan Inst. Chem. Eng.* **2022**, *132*, No. 104110.

(31) Simon, P.; Gogotsi, Y. Materials for electrochemical capacitors. *Nat. Mater.* **2008**, *7*, 845−854.

(32) Lyu, W.; Yan, C.; Chen, Z.; Chen, J.; Zuo, H.; Teng, L.; Liu, H.; Wang, L.; Liao, Y. Spirobifluorene-Based Conjugated Microporous Polymer-Grafted Carbon Nanotubes for Efficient Supercapacitive Energy Storage. *ACS Appl. Energy Mater.* **2022**, *5*, 3706−3714.

(33) Mohamed, M. G.; Chen, T. C.; Kuo, S. W. Solid-State Chemical Transformations to Enhance Gas Capture in Benzoxazine-Linked Conjugated Microporous Polymers. *Macromolecules* **2021**, *54*, 5866−5877.

(34) Yu, K.; Pan, X.; Zhang, G.; Liao, X.; Zhou, X.; Yan, M.; Xu, L.; Mai, L. Nanowires in Energy Storage Devices: Structures, Synthesis, and Applications. *Adv. Energy Mater.* **2018**, *8*, No. 1802369.

(35) Samy, M. M.; Mohamed, M. G.; El-Mahdy, A. F. M.; Mansoure, T. H.; Wu, K. C. W.; Kuo, S. W. High-Performance Supercapacitor Electrodes Prepared From Dispersions of Tetrabenzonaphthalene-Based Conjugated Microporous Polymers and Carbon Nanotubes. *ACS Appl. Mater. Interfaces* **2021**, *13*, 51906−51916.

(36) Bruce, P. G.; Scrosati, B.; Tarascon, J. M. Nanomaterials for Rechargeable Lithium Batteries. *Angew. Chem., Int. Ed.* **2008**, *47*, 2930−2946.

(37) Liao, Y.; Wang, H.; Zhu, M.; Thomas, A. Efficient Supercapacitor Energy Storage Using Conjugated Microporous Polymer Networks Synthesized from Buchwald−Hartwig Coupling. *Adv. Mater.* **2018**, *30*, No. 1705710.

(38) Lin, Z.; Goikolea, E.; Balducci, A.; Naoi, K.; Taberna, P. L.; Salanne, M.; Yushin, G.; Simon, P. Materials for Supercapacitors: When Li-Ion Battery Power is not Enough. *Mater. Today* **2018**, *21*, 419−436.

(39) Mohamed, M. G.; Mansoure, T. H.; Samy, M. M.; Takashi, Y.; Mohammed, A. A. K.; Ahamad, T.; Alshehri, S. M.; Kim, J.; Matsagar, B. M.; Wu, K. C. W.; Kuo, S. W. Ultrastable Conjugated Microporous Polymers Containing Benzobisthiadiazole and Pyrene Building Blocks for Energy Storage Applications. *Molecules* **2022**, *27*, 2025.

(40) Chen, D.; Jiang, K.; Huang, T.; Shen, G. Recent Advances in Fiber Supercapacitors: Materials, Device Configurations, and Applications. *Adv. Mater.* **2020**, *32*, No. 1901806.

(41) Manjunatha, N.; Imadadulla, M.; Lokesh, K. S.; Reddy, K. R. Synthesis and electropolymerization of tetra-[β-(2-benzimidazole)] and tetra-[β-(2-(1-(4- aminophenyl))benzimidazole)] embedded cobalt phthalocyanine and their supercapacitance behaviour. *Dyes Pigm.* **2018**, *153*, 213−224.

(42) Wang, Y. G.; Song, Y. F.; Xia, Y. Y. Electrochemical capacitors: mechanism, materials, systems, characterization and applications. *Chem. Soc. Rev.* **2016**, *45*, 5925−5950.

(43) Mohamed, M. G.; Sharma, S. U.; Liu, N. Y.; Mansoure, T. H.; Samy, M. M.; Chaganti, S. V.; Chang, Y. L.; Lee, J. T.; Kuo, S. W. Ultrastable Covalent Triazine Organic Framework Based on Anthracene Moiety as Platform for High-Performance Carbon Dioxide Adsorption and Supercapacitors. *Int. J. Mol. Sci.* **2022**, *23*, 3174.

(44) Mohamed, M. G.; Sharma, S. U.; Yang, C. H.; Samy, M. M.; Mohammed, A. A. K.; Chaganti, S. V.; Lee, J. T.; Kuo, S. W. Anthraquinone-Enriched Conjugated Microporous Polymers as Organic Cathode Materials for High-Performance Lithium-Ion Batteries. *ACS Appl. Energy Mater.* **2021**, *4*, 14628−14639.

(45) Mohamed, M. G.; Samy, M. M.; Mansoure, T. H.; Sharma, S. U.; Tsai, M. S.; Chen, J. H.; Lee, J. T.; Kuo, S. W. Dispersions of 1,3,4-Oxadiazole-Linked Conjugated Microporous Polymers with Carbon Nanotubes as a High-Performance Electrode for Supercapacitors. *ACS Appl. Energy Mater.* **2022**, *5*, 3677−3688.

(46) Meng, N.; Ren, X.; Santagiuliana, G.; Ventura, L.; Zhang, H.; Wu, J.; Yan, H.; Reece, M. J.; Bilotti, E. Ultrahigh β-phase content poly(vinylidene fluoride) with relaxor-like ferroelectricity for high energy density capacitors. *Nat. Commun.* **2019**, *10*, No. 4535.

(47) EL-Mahdy, A. F. M.; Yu, T. C.; Mohamed, M. G.; Kuo, S. W. Secondary Structures of Polypeptide-Based Diblock Copolymers Influence the Microphase Separation of Templates for the Fabrication of Microporous Carbons. *Macromolecules* **2021**, *54*, 1030−1042.

(48) Luo, L. W.; Zhang, C.; Xiong, P.; Zhao, Y.; Ma, W.; Chen, Y.; Zeng, J. H.; Xu, Y.; Jiang, J. X. A redox-active conjugated microporous polymer cathode for high-performance lithium/potassium-organic batteries. *Sci. China: Chem.* **2021**, *64*, 72−81.

(49) Son, H.; Yang, M. H.; Mutyala, A. K.; Chang, D. W.; Park, J. S. Superior electrocatalytic performance of polyisobutylene-substituted metallophthalocyanines supported on single-walled carbon nanotubes for an oxygen reduction reaction. *Dyes Pigm.* **2019**, *162*, 662−670.

(50) Feng, E.; Ma, G. F.; Peng, H.; Hua, F. T.; Tang, W.; Lei, Z. Sponge integrated highly compressible all-solid-state supercapacitor with superior performance. *New J. Chem.* **2017**, *41*, 13347−13354.

(51) Khalid, M.; Varela, H. A general potentiodynamic approach for red phosphorus and sulfur nanodot incorporation on reduced graphene oxide sheets: metal-free and binder-free electrodes for supercapacitor and hydrogen evolution activities. *J. Mater. Chem. A* **2018**, *6*, 3141−3150.

(52) Cao, J. Y.; Zhao, Y.; Xu, Y. F.; Zhang, Y.; Zhang, B.; Peng, H. S. Sticky-note supercapacitors. *J. Mater. Chem. A* **2018**, *6*, 3355−3360.

(53) Zhang, H. H.; Zhang, Y. N.; Gu, C.; Ma, Y. G. Electropolymerized conjugated microporous poly(zinc-porphyrin) films as potential electrode materials in supercapacitors. *Adv. Energy Mater.* **2015**, *5*, No. 1402175.

(54) Ahn, H.; Huang, Y. C.; Lin, C. W.; Lee, Y. H.; et al. Efficient defect healing of transition metal dichalcogenides by metallophthalocyanine. *ACS Appl. Mater. Interfaces* **2018**, *10*, 29145−29152.

(55) Bıyıklıoğlu, Z.; Çakır, V.; Koca, A.; Kantekin, H. Synthesis, electrochemical, in-situ spectroelectrochemical and in-situ electrocolorimetric characterization of nonperipheral tetrasubstituted metal-free and metallophthalocyanines. *Dyes Pigm.* **2011**, *89*, 49−55.

(56) Halder, A.; Meena, G.; Abdul, K. M.; Saibal, B.; et al. Interlayer hydrogen-bonded covalent organic frameworks as high-performance supercapacitors. *J. Am. Chem. Soc.* **2018**, *140*, 10941−10945.

(57) Cai, T. L.; Wang, H. W.; Jin, C. D.; Sun, Q. F.; Nie, Y. J. Fabrication of nitrogen-doped porous electrically conductive carbon aerogel from waste cabbage for supercapacitors and oil/water separation. *J. Mater. Sci. Mater. Electron.* **2018**, *29*, 4334−4344.

(58) Liu, X.; Xu, Y.; Guo, Z.; Nagai, A.; Jiang, D. Super absorbent conjugated microporous polymers: a synergistic structural effect on the exceptional uptake of amines. *Chem. Commun.* **2013**, *49*, 3233−3235.

(59) Fischer, S.; Schimanowitz, A.; Dawson, R.; Senkovska, I.; Kaskel, S.; Thomas, A. Cationic Microporous Polymer Networks by Polymerisation of Weakly Coordinating Cations with CO$_2$-Storage Ability. *J. Mater. Chem. A* **2014**, *2*, 11825−11829.

(60) Wang, H.; Cheng, Z.; Liao, Y.; Li, J.; Weber, J.; Thomas, A.; Faul, C. F. J. Conjugated Microporous Polycarbazole Networks as Precursors for Nitrogen-Enriched Microporous Carbons for CO$_2$ Storage and Electrochemical Capacitors. *Chem. Mater.* **2017**, *29*, 4885−4893.

(61) Hu, J.; Zhang, D.; Harris, F. W. Ruthenium(III) Chloride Catalyzed Oxidation of Pyrene and 2,7-Disubstitued Pyrenes: An Efficient, One-Step Synthesis of Pyrene-4,5-diones and Pyrene-4,5,9,10-tetraones. *J. Org. Chem.* **2005**, *70*, 707−708.

(62) Cui, H.; Hu, P.; Zhang, Y.; Huang, W.; Li, A. Research Progress of High-Performance Organic Material Pyrene-4,5,9,10-Tetraone in Secondary Batteries. *ChemElectroChem* **2021**, *8*, 352−359.

(63) Nokami, T.; Matsuo, T.; Inatomi, Y.; Hojo, N.; Tsukagoshi, T.; Yoshizawa, H.; Shimizu, A.; Kuramoto, H.; Komae, K.; Tsuyama, H.; Yoshida, J. I. Polymer-Bound Pyrene-4,5,9,10-tetraone for Fast-Charge and -Discharge Lithium-Ion Batteries with High Capacity. *J. Am. Chem. Soc.* **2012**, *134*, 19694−19700.

(64) Zheng, S.; Miao, L.; Sun, T.; Li, L.; Ma, T.; Bao, J.; Tao, Z.; Chen, J. An extended carbonyl-rich conjugated polymer cathode for high-capacity lithium-ion batteries. *J. Mater. Chem. A* **2021**, *9*, 2700−2705.

(65) Mohamed, M. G.; Elsayed, M. H.; Elewa, A. M.; EL-Mahdy, A. F. M.; Yang, C. H.; Mohammed, A. A. K.; Chou, H. H.; Kuo, S. W. Pyrene-containing conjugated organic microporous polymers for photocatalytic hydrogen evolution from water. *Catal. Sci. Technol.* **2021**, *11*, 2229−2241.

(66) Mohamed, M. G.; Tsai, M. Y.; Wang, C. F.; Huang, C. F.; Danko, M.; Dai, L.; Chen, T.; Kuo, S. W. Multifunctional Polyhedral Oligomeric Silsesquioxane (POSS) Based Hybrid Porous Materials for CO$_2$ Uptake and Iodine Adsorption. *Polymers* **2021**, *13*, 221.

(67) Salunkhe, R. R.; Zakaria, M. B.; Kamachi, Y.; Alshehri, S. M.; Ahamad, T.; Torad, N. L.; Dou, S. X.; Kim, J. H.; Yamauchi, Y. Fabrication of asymmetric supercapacitors based on coordination polymer derived nanoporous materials. *Electrochim. Acta* **2015**, *183*, 94−99.

(68) Sharma, V.; Sahoo, A.; Sharma, Y.; Mohanty, P. Synthesis of nanoporous hypercrosslinked polyaniline (HCPANI) for gas sorption and electrochemical supercapacitor applications. *RSC Adv.* **2015**, *5*, 45749−45754.

(69) Abdelhamid, H. N.; Al Kiey, S. A.; Sharmoukh, W. A high-performance hybrid supercapacitor electrode based on ZnO/nitrogen-doped carbon nanohybrid. *Appl. Organomet. Chem.* **2022**, *36*, No. e6486.

(70) Sengottaiyan, C.; Jayavel, R.; Shrestha, R. G.; Subramani, T.; Maji, S.; Kim, J. H.; Hill, J. P.; Ariga, K.; Shrestha, L. K. Indium Oxide/Carbon Nanotube/Reduced Graphene Oxide Ternary Nanocomposite with Enhanced Electrochemical Supercapacitance. *Bull. Chem. Soc. Jpn.* **2019**, *92*, 521−528.

▢ Recommended by ACS